

BEAM DIAGNOSTICS AT THE HAMBURG ISOCHRONOUS CYCLOTRON BY ION TIME-OF-FLIGHT MEASUREMENTS ⁺⁾

H. Krause, R. Langkau, W. Peters, N. Schirm and W. Scobel

University of Hamburg, I. Institute for Experimental Physics, Cyclotron Laboratory, Luruper Chaussee 149, D-2000 Hamburg 50, Federal Republic of Germany

Abstract.— Time-of-flight measurements for the internal beam pulses in a cyclotron reveal interesting and important features of the internal beam dynamics. Especially in the case of strongly overlapping pulses this technique is a valuable diagnostic tool. The following article gives a simplified discussion of the method and presents first results obtained at the Hamburg Isochronous Cyclotron.

1. Introduction.— The Hamburg Isochronous Cyclotron was designed for high output currents. Among other things this has been achieved by accepting ions out of a rather large phase angle interval of about $\Delta\varphi = 30^\circ\text{--}40^\circ$ into the acceleration process which inevitably causes a corresponding large radial width of the internal beam pulses. At radii greater than about one half the extraction radius of $R_E = 560$ mm no orbit separation can be observed in differential current measurements. Thus the only possibility of localizing the radial position of individual orbits and getting information about their radial shape is the measurement of the time-of-flight of the ions (respectively of the beam pulses) from the center of the cyclotron to an internal target with a well known radial position R .

In the conduct of a research project at the Hamburg Isochronous Cyclotron for the improvement of the internal and external beam quality and the extraction conditions such time-of-flight measurements were started for radii r in the vicinity of R_E .

2. Experimental setup.— A schematic diagram of the experimental setup is given in figure 1: An axial electric deflector D on the first orbit works as a gate for the beam pulses BP from the ion source I . It is held closed by a sufficiently high bias voltage supplied by BV and is opened by the output pulses of a pulse generator and power stage PG . These pulses are properly timed with respect to the RF phase and switch off the bias voltage. PG is triggered by the cyclotron RF via a frequency divider FD which scales down the original frequency far enough to prevent radial overlapping of the beam pulses released by D into the further acceleration process.

The time of arrival of the beam pulse BP at the radius R is indicated by the emission of gamma radiation from the interaction of the ions with an integral target T whose radial position is controlled by a target step motor TSM . The gamma radiation is detected by a fast scintillation counter SC whose output pulses serve as stop signals for a time-to-pulse height converter TPC after being shaped by a timing pulse former PF . The start pulses for the TPC are taken from PG . The spectra are stored in a multichannel analyzer MCA .

3. Theoretical considerations.— The time spectra $S(R,t)$ obtained in that way are determined by the radial motion of the beam pulse across the front edge of the target and in particular reveal the influence of coherent radial oscillations on that motion. Fig. 2 schematically illustrates the basic facts: $F_0(r)$ describes the radial shape of an internal beam pulse under observation on a turn number $N=N_0$ at the time $t=t_0$. Both coordinates may

arbitrarily be chosen as $N_0=0$ and $t_0=0$.

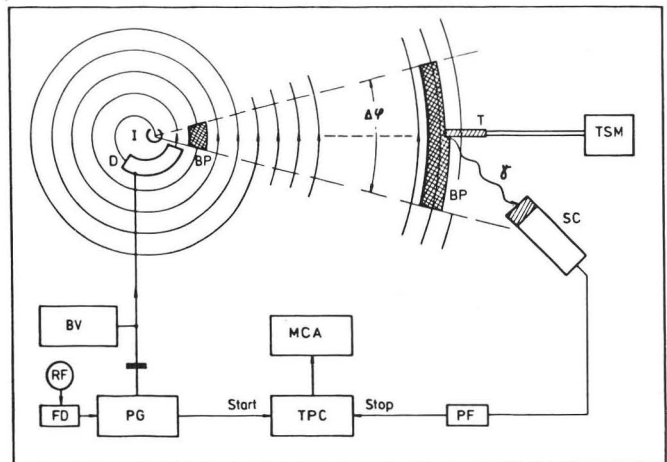


Fig. 1: Experimental setup (schematic).

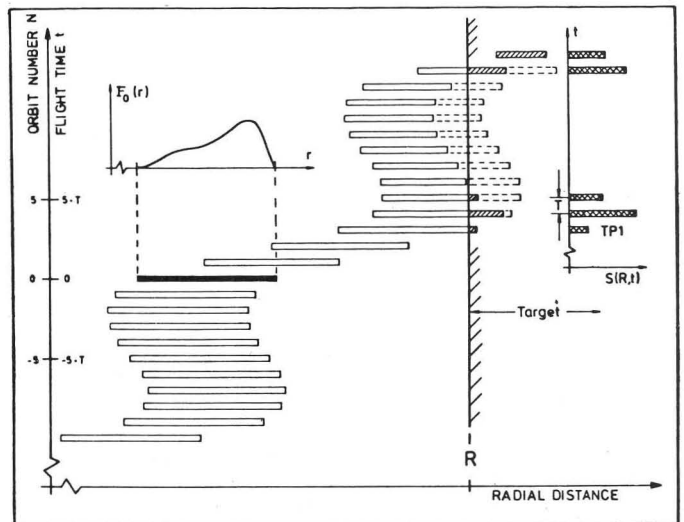


Fig. 2: Schematic history of a beam pulse under coherent radial oscillations and its interaction with an integral target at position R .

^{+) Work supported by the "Bundesministerium für Forschung und Technologie"}

Under the simplifying assumption that the pulse maintains its shape within the region of interest its radial motion along a constant azimuth is given by:

$$F(r,t) = F_0(r-v \cdot t).$$

The time is a discrete variable $t = N \cdot T$ where in a one-dee-cyclotron T is the RF-period. The velocity v is:

$$v = \frac{dr}{dt} = \frac{\Delta r(N)}{T}$$

where $\Delta r(N)$ is the radial shift of the beam pulse on the N -th turn. This yields:

$$F(r,t=N \cdot T) = F_0[r-N \cdot \Delta r(N)] = F(r,N).$$

An integral target at the position $r=R$ peels off the fraction:

$$f(R,N) = F(R,N) \cdot \Delta r(N) = F_0[R-N \cdot \Delta r(N)] \cdot \Delta r(N)$$

of the beam pulse per turn.

If $F = dP/dr$ means the radial density of the number P of ions in the beam pulse then

$$f = \frac{dP}{dr} \cdot \Delta r = \Delta P$$

is the number of ions hitting the target per turn. At constant ion energy the number Γ of gamma quanta emitted by the target is proportional to P . Thus a time spectrum $S(R,t)$ consists of a series of time peaks of equal width proportional to $\Delta \varphi$ and equally spaced by the RF-period T where the intensity of each peak is proportional to the number $\Delta \Gamma$ of gamma quanta emitted per turn and thus proportional to ΔP respectively f :

$$S(R,t) = S(R,N) \sim F_0[R-N \cdot \Delta r(N)] \cdot \Delta r(N).$$

The radial shift per turn $\Delta r(N)$ is the sum of two components:

$$\Delta r(N) = dr(N) + \delta r(N).$$

$dr(N)$ is the radial gain per turn due to acceleration and

$$\begin{aligned} \delta r(N) &= 2 \cdot \pi \cdot (\nu_r - 1) \cdot A \cdot \sin[2 \cdot \pi \cdot (\nu_r - 1) \cdot N] \\ &= \delta_m \cdot \sin[2 \cdot \pi \cdot (\nu_r - 1) \cdot N] \end{aligned}$$

is the radial shift per turn due to coherent radial oscillations where ν_r is the frequency number, A the amplitude of the oscillation and $\delta_m = 2 \cdot \pi \cdot (\nu_r - 1) \cdot A$ the amplitude of δr . $\delta r(N)$ is negative during that half period of the oscillation, where the orbit center moves backward.

a.) For $dr(N) > \delta_m$ or $A < dr(N)/2 \cdot \pi \cdot (\nu_r - 1)$, that is for "small" amplitudes A , the total shift $\Delta r(N)$ is positive throughout the oscillation period containing $\Delta N = 1/(\nu_r - 1)$ turns. This means that the leading edge

of the beam pulse is gradually and monotonically shifted outwards with each additional turn. The total number of peaks in $S(R,t)$ is equal to the number of turns necessary to push the whole beam pulse across the target edge. Figures 3 and 4 show calculated spectra $S(R,t)$ for the case $dr(N) > \delta_m$ under various conditions. The pulse shape $F_0(r)$ used in these calculations is an asymmetric Gaussian function with a steep leading and a flat trailing edge (cf. figure 2):

$$F_0(r) = \exp \left[\frac{(r_0 - r)^2}{a^2} \right] \quad \text{for } r > r_0 \quad \text{and}$$

$$F_0(r) = \exp \left[\frac{(r_0 - r)^2}{(4a)^2} \right] \quad \text{for } r < r_0.$$

This function appears as the envelope of the first spectrum in figure 3. The individual time peaks are indicated as bars spaced by T .

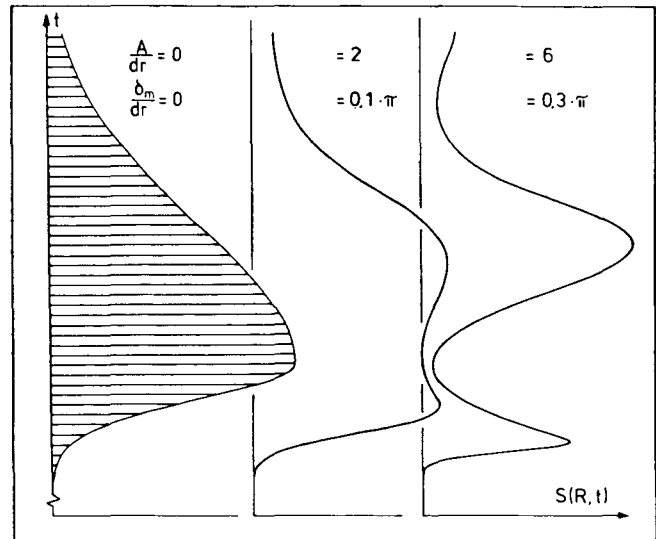


Fig. 3: Calculated time spectra for three different oscillation amplitudes.

The three spectra of figure 3 refer to the same target position R , the same frequency number $\nu_r = 1,025$ and three different oscillation amplitudes A relative to $dr(N)$, whose values are marked in the diagram. The second and third spectra are represented by their envelopes only.

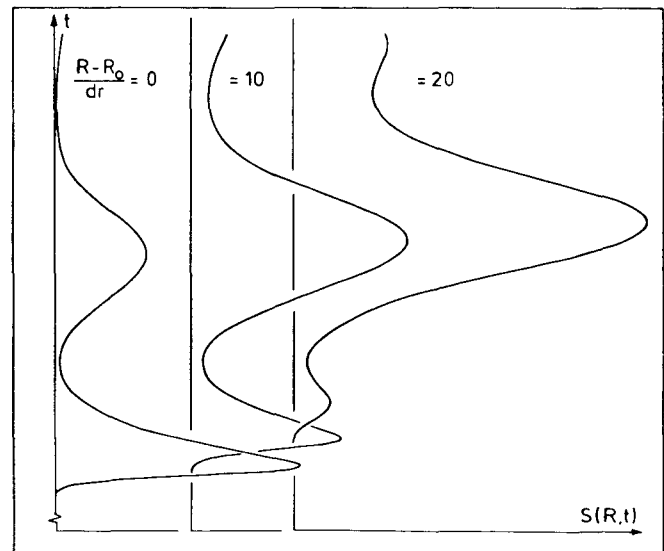


Fig. 4: Calculated time spectra for three different radial positions R of the integral target.

The three time spectra of figure 4 again plotted as their envelopes refer to the same amplitude $A = 6 \cdot dr(N)$ and to three different target positions R with respect to a reference position R_0 given in units of $dr(N)$.

A comparison clearly shows the remarkable feature that the initial bump decreases and the following one increases as the target steps outward that means as R increases. This feature (cf. figure 2) can be traced back to the fact that from $R=R_0$ to $R = R_0 + 20 \cdot dr$ the target approaches the leading edges of the beam pulses on those turns where $\delta r(N)$ during the negative half period of the oscillation begins to compensate $dr(N)$ significantly.

b.) For $dr(N) < \delta_m$ or $A > dr(N) / 2 \cdot \pi \cdot (v_r - 1)$, that is for "large" amplitudes A, the shift $\Delta r(N)$ becomes negative for $\Delta N_- = N_2 - N_1$ turns during the backward motion of the orbit centers in a region around the negative amplitude δ_m between the limits given by $dr(N_1) = -\delta r(N_1)$ and $dr(N_2) = -\delta r(N_2)$. If dr , A and v_r are assumed to be constant within that interval the number of orbits within these limits follows from:

$$\Delta N_- = \frac{1}{\pi \cdot (v_r - 1)} \cdot \cos^{-1} \frac{dr}{2 \cdot \pi \cdot (v_r - 1) \cdot A}$$

ΔN_- thus depends on the ratio dr/A . The peaks belonging to these orbits do not appear in the time spectrum $S(R,t)$, because the beam pulses on these orbits move away from the target edge. $S(R,t)$ thus separates into two (or even more) groups of peaks. If v_r is known the ratio dr/A may be computed from the observed number ΔN_- of these "missing peaks" by:

$$\frac{dr}{A} = 2 \cdot \pi \cdot (v_r - 1) \cdot \cos \left[\pi \cdot (v_r - 1) \cdot \Delta N_- \right] \quad (A)$$

4. Experimental results.- The first measurements to test the usefulness of the method explained above were performed with protons accelerated to a final energy of 20 MeV. Time spectra $S(R,t)$ were taken for target positions R between 490 and 540 mm in $\Delta R = 1,0$ mm steps. Figure 5 shows three selected and typical spectra plotted as bar diagrams.

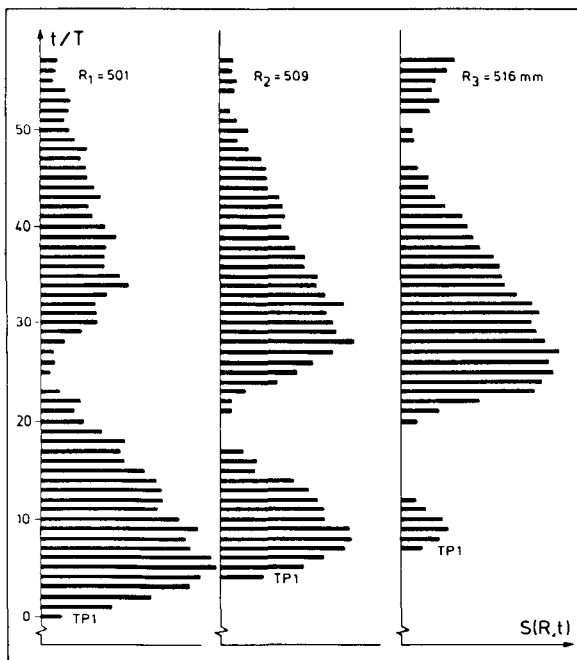


Fig. 5: Measured time spectra for three different radial positions R of the integral target (protons; 20 MeV).

Their structure qualitatively follows that one predicted by the calculations. The corresponding target positions R_1 , R_2 and R_3 are marked in figure 6. The large modulation depth observed indicates large oscillation amplitudes.

The first time peak of each spectrum $S(R,t)$ labelled by TP1 in figure 5 marks the outer boundary or leading edge of the beam pulse $F(r,N)$ under observation. Figure 6 shows a plot of the time t_1 for TP1 versus r. Every drop in t_1 by one RF period T means that the target, moving inwards, has touched the beam pulse on a preceding orbit. The projection of these steps in t_1 onto the r-axis thus yields the radial distribution of the leading edges of the beam pulses on their successive orbits.

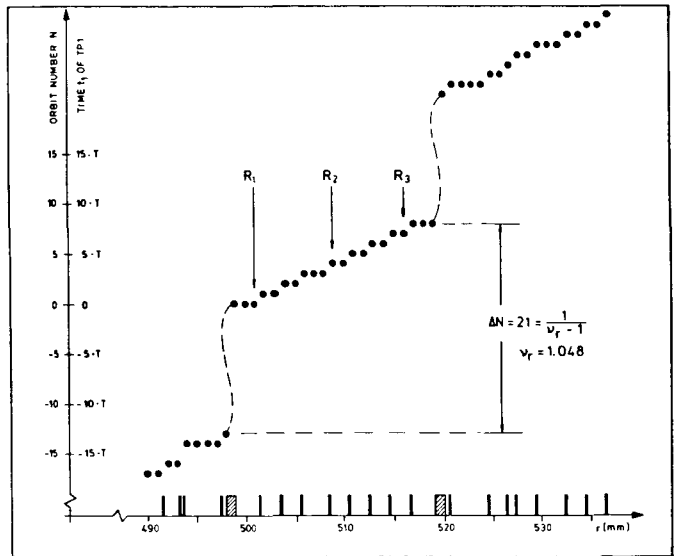


Fig. 6: Radial distribution of the leading edges of the internal beam pulses (protons; 20 MeV).

The large gaps in t_1 around $r = 498$ mm and $r = 519$ mm are caused by the backbending of the beam pulse position due to the large amplitudes A. These areas are not accessible by the technique presented here. Nevertheless the number ΔN of turns for a complete oscillation period can be counted from figure 6 so that the frequency number v_r can be determined accurately.

$\Delta N = 21$ yields $v_r = 1 + 1/\Delta N = 1,048$. This makes it possible to evaluate the ratios dr/A from equation (A) by taking the numbers ΔN_- of missing peaks from the measured time spectra. If in addition dr is calculated from the nonrelativistic formula:

$$dr = \frac{c^2 \cdot T^2}{4 \cdot \pi^2 \cdot v_r^2} \cdot \frac{dE}{E_0} \cdot \frac{1}{r}$$

where dE is the energy gain per turn, E_0 the proton rest energy and c the velocity of light, then the amplitudes A can be obtained. This is a sufficiently accurate approximation at the energies considered here. As an example the following table summarizes the results from the spectra of figure 5.

R [mm]	ΔN_-	dr [mm]	A [mm]
501	1	0,83	2,8
509	3	0,81	3,0
516	7	0,80	5,4

The increase of A with r might be due to the approach towards the $\nu_r=1$ resonance at about $r = 540$ mm.

Radial oscillation amplitudes can be determined in a well known manner by shadow measurements. According to the procedures worked out by Richardson ¹⁾ or Garren and Smith ²⁾ A can be evaluated from the diffuseness of a current shadow cast by a sharp edged target located upstream on an earlier azimuth. Figure 7 shows examples of shadow curves for three positions R of the target obtained in earlier measurements at our cyclotron (protons; final energy: 20 MeV).

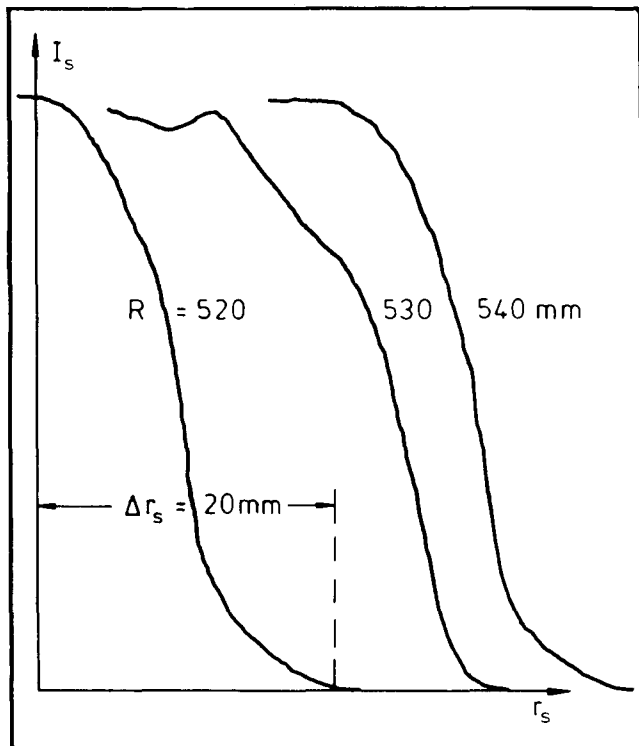


Fig. 7: Shadow curves (protons; 20 MeV).

$I_s(r_s)$ is the internal current measurement on a second integral target 190° downstream. The observed diffuseness of $\Delta r_s = 20$ mm yields an amplitude of about $A = 5$ to 7 mm at $R = 520$ mm in fairly good agreement with the value given in the table above.

In summarizing it should be emphasized that the numerical results and conclusions drawn from the measurements and discussions are only as accurate and reliable as the restrictions and approximations applied permit and are valid as long as the motion of the internal beam pulses can be represented in the simple way sketched in figure 2. Nevertheless the method presented here supplements other existing diagnostic methods and is the only one to get more direct information on orbit dynamics in the case of strongly overlapping beam pulses.

Further improvements of the method and its applications for diagnostic purposes at our cyclotron are in progress.

We gratefully acknowledge the support by the "Bundesministerium für Forschung und Technologie" and the assistance of Dr. Lezoch in the calculations.

References

1. J.R. Richardson, Progress in Nuclear Techniques and Instrumentation, Vol. 1, North Holland Publ. Company (1965)
2. A.A. Garren and L. Smith, Proc. Conf. SF Cyclotrons, CERN 63-19, 18 (1963)

" DISCUSSION "

M.F. FINLAN : What is deflector voltage ?

R. LANGKAU : ~ 1 kV. For details see: Nucl. Instr. & Meth. 134 (1976) 15.

H.W. SCHREUDER : If I understood you correctly, your time-of-flight measurements give you the oscillation of the beam as a whole, that is to say, the coherent oscillation. On the other hand, I think that the width of the beam shadow gives you the incoherent oscillation. Would you comment on that ?

R. LANGKAU : We tried to work out the coherent part of the oscillations on the basis of the procedures described by RICHARDSON, GARREN and SMITH. The amplitudes taken from the shadow measurements represent a rough estimate.

D.A. DOHAN : We have used a technique similar to this to count turns during our separated turn operation. I have a question : what sort of magnetic field tolerances or stability do you need or did you have in these measurements, and how does the stability affect your results ?

R. LANGKAU : The stability of the magnetic field in our measurements was better than $\Delta B/B = 10^{-5}$.

D.A. DOHAN : We have used a technique similar to this to count turns during our separated turn operation. I have a question : what sort of magnetic field tolerances or stability do you need or did you have in these measurements and how does the stability affect your results ?

R. LANGKAU : The stability of the magnetic field in our measurements was better than $\Delta B/B = 10^{-5}$.